

# Investigation in modelling piping erosion with a coupled « lattice Boltzmann – discrete element » numerical method

Luc SIBILLE<sup>1</sup>, Franck LOMINÉ<sup>2</sup>, Didier MAROT<sup>1</sup>

<sup>1</sup>GeM laboratory, l'Université Nantes Angers Le Mans - LUNAM -, CNRS  
IUT de Saint Nazaire, BP 420, 44606 Saint-Nazaire Cedex, France – luc.sibille@univ-nantes.fr

<sup>2</sup>Université Européenne de Bretagne – INSA, LGCGM, EA3913  
20, Avenue des Buttes de Coësmes, CS 70839, 35708 Rennes Cedex 7, France – franck.lomine@insa-rennes.fr

*A coupled fluid-solid numerical method is presented. The solid phase consists of a granular assembly where dynamics of each solid particle is described with the discrete element method. In the inter-particle space the fluid flow is solved with the lattice Boltzmann method. Interactions between the solid phase and the fluid phase result from the integration, over the solid particle boundary, of the momentum exchange between solid and fluid phases. Consequently, assumptions about fluid-solid interactions are very limited with such a coupling.*

*To illustrate abilities and limits of the coupled method in the framework of internal soil erosion, a two-dimensional model of piping erosion is considered (inspired from the hole erosion test). Direct simulations of erosion of a cohesive-frictional granular matter have been performed for different values of water pressure gradient and inter-particle cohesion. As classically found experimentally, the mass rate of erosion follows a relation of the kind of Shield's law, with a linear dependency on the hydraulic shear stress. A critical hydraulic shear stress, below which detachment of particles does not occur, can be identified and is directly related to the inter-particle cohesion. On the contrary, this latter has no influence on the erosion coefficient.*

## Key words

Piping erosion, discrete element method, lattice Boltzmann method, fluid-solid coupling, granular matter.

## I INTRODUCTION

Experimental observation and characterization of internal soil erosion at the scale of soil particles constitute a difficult task even if some techniques, using for instance analogue granular material [Tsai, 2003], could offer such possibilities. Nevertheless a description and characterisation of internal erosion at the microscopic scale (i.e. at the scale of soil particles or aggregates) could be complementary to the macroscopic description obtained from more conventional experimental devices, and would help in the identification of the key parameters fixing the erosion regime.

In this context, we present in this paper a coupled numerical method where a two-phase (solid/fluid) granular assembly is described at the microscopic scale [Lominé, 2012]. Each particle or aggregate of the solid granular phase is explicitly described through the discrete element method (DE method) [Cundall, 1979] where positions and velocities of solid particles results from the explicit time integration of Newton's law. The fluid phase dynamics in the inter-particle space is solved with the lattice Boltzmann method (LB method) [Succi, 2001]. DE and LB methods are fully coupled. Since the step of the spatial discretization of the fluid phase is chosen sufficiently small to describe full fields of velocity and pressure (actually in the LB method this consists in a full field of particle distribution functions) around solid particles, interactions between the solid and fluid phases result simply from the integration, over the solid boundaries, of the momentum exchange between solid and fluid phases. Consequently, assumptions about fluid-solid interactions are very limited with such a coupling. For instance, and contrary to some other methods, permeability and drag forces result from the coupling and are not introduced *a priori*. Both numerical methods and their coupling are briefly presented in the first section of the paper.

Generally speaking, internal erosion in soil can involve three different steps: particle detachment, transport and possibly filtration. For each of these steps, description and characterisation at particle scale of physical

phenomena constitutes a challenging point. Consequently, to proceed gradually, we have chosen to focus, at first, on the particle detachment step. To avoid to deal with the transport of detached particles (in the interstitial space) and their filtration, we developed a numerical model inspired from the hole erosion test (HET) [Wan, 2004]. This model, constitutes an heuristic two-dimensional case of piping erosion with a pre-existing hole from where particle detachment occurs. Direct simulations are carried out as numerical experiments and interpreted in a similar way as the one classically followed for the hole erosion test [Wan, 2002]. Numerical model, simulations and parametric studies are presented in a second section of the paper.

## II THE COUPLED LB-DE NUMERICAL METHOD

A detailed description of the coupled method can be found in [Lominé, 2012]. The numerical coupling has been implemented in the open-source software YADE [Šmilauer, 2010] constituting a general framework for discrete numerical models.

### II.1 The lattice Boltzmann (LB) method

The description of the water flow is based on the resolution of the lattice Boltzmann equation with the simplified Bhatnagar-Gross-Krook collision operator [Bhatnagar, 1954], aiming to represent the space and time evolution of the distribution function (or probability density)  $f(\vec{x}, t)$ . Such function represents the probability of finding fluid particles (or molecules) around a position  $\vec{x}$  at a time  $t$  and with a given momentum. The whole simulation domain (including the fluid space and the solid particles) is discretized following the classical two-dimensional D2Q9 model [Qian, 1992], consisting in a regular square lattice of step  $h$  with nine directions of propagation of fluid particles (see Figure 1-a). From a given node of the lattice, eight of these propagation directions numbered by  $i = 1, 2, 3 \dots 8$  point towards the eight first neighbouring nodes, whereas the ninth direction numbered  $i = 0$  point toward the considered node itself, representing still particles. Consequently nine components  $f_i(\vec{x}, t)$  (with  $i = 1$  to 9) of the distribution function can be distinguished.

The application of the LB method consists in an iterative process over time. Each numerical time step  $dt$  is split into a collision stage and a propagation stage. During the collision stage, fluid particles collide according to the BGK operator (which can be seen as a linearization of the collision operator originally defined in the Boltzmann equation):

$$f_i(\vec{x}, t^+) = f_i(\vec{x}, t) - \frac{1}{\tau} [f_i(\vec{x}, t) - f_i^{eq}(\vec{x}, t)], \quad (1)$$

where  $t^+$  denotes the post-collision time,  $\tau$  is a dimensionless relaxation time related to the kinematic viscosity of the fluid  $\nu$ , and  $f_i^{eq}$  is an equilibrium distribution function parameterized by the macroscopic fluid velocity  $\vec{v}$  and density  $\rho$  at the considered node. For a Newtonian fluid the equilibrium distribution function writes:

$$f_i^{eq} = w_i \rho \left( 1 + \frac{3}{C^2} \vec{e}_i \cdot \vec{v} + \frac{9}{2C^4} (\vec{e}_i \cdot \vec{v})^2 + \frac{3}{2C^2} \vec{v} \cdot \vec{v} \right), \quad (2)$$

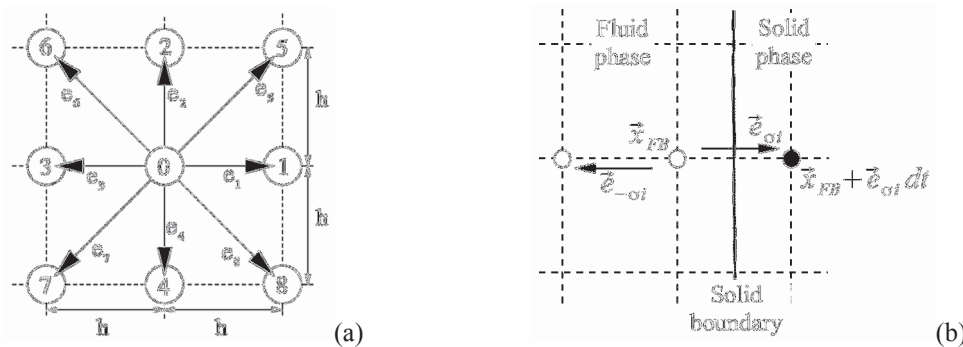


Figure 1: Lattice and particle discrete velocities  $e_i$  defined in the D2Q9 model used in the LB method (a), and definition of a boundary link  $\sigma_i$  (b).

with  $w_0 = 4/9$ ,  $w_{1,2,3,4} = 1/9$ , and  $w_{5,6,7,8,9} = 1/36$  for the D2Q9 model;  $C = h/dt$ , the lattice velocity; and  $\vec{e}_i$  the discrete propagation velocities associated to the D2Q9 model and defined by:

$$\vec{e}_i = \begin{cases} (0,0) & \text{if } i = 0 \\ C \left( \cos \frac{\pi(i-1)}{2}, \sin \frac{\pi(i-1)}{2} \right) & \text{for } i = 1, \dots, 4 \\ \sqrt{2}C \left( \cos \frac{\pi(2i-9)}{4}, \sin \frac{\pi(2i-9)}{4} \right) & \text{for } i = 5, \dots, 8 \end{cases} \quad (3)$$

The propagation stage is performed after the collision stage to transport, at the end of time step  $dt$ , the post-collision distribution functions to the neighbouring nodes according to the discrete velocities  $\vec{e}_i$  such that:

$$f_i(\vec{x} + \vec{e}_i dt, t + dt) = f_i(\vec{x}, t^+), \quad (4)$$

where  $\vec{x} + \vec{e}_i dt$  represents for the node at position  $\vec{x}$  the nearest neighbouring node along the  $i$ -th direction.

Finally, macroscopic fluid density and velocity can be retrieved at each node with:

$$\rho = \sum_{i=0}^8 f_i \quad \text{and} \quad \vec{v} = \frac{1}{\rho} \sum_{i=0}^8 f_i \vec{e}_i, \quad (5)$$

In the LB method the fluid is considered as slightly compressible and the fluid pressure  $p$  is related to its density  $\rho$  through the state equation  $p = c_s^2 \rho$ , where  $c_s = C/\sqrt{3}$  is the sound celerity. For sufficiently small Mach number  $M = v_{\max}/C$  (where  $v_{\max}$  is the highest flow velocity), typically lower than 0.1, fluid compressibility stays negligible and fluid velocity and pressure converge to the solution of the incompressible Navier-Stokes equation.

## II.2 The discrete element (DE) method

Dynamic of the solid granular packing is described with the discrete element method as introduced by [Cundall, 1979]. Here solid particles are represented by two-dimensional discs and the mechanical parameters for the solid phase are introduced at the inter-particle contact scale.

Contact interaction forces are computed for each couple of contacting particles according to a cohesive frictional contact law presented in Figure 2. To linearise the contact law, contacting particles can slightly overlap, this overlap is denoted  $\delta_n$ . In the normal direction to the tangent to the contact, the relation between the normal contact force  $F_n$  and  $\delta_n$  is purely elastic and characterised by a normal stiffness  $k_n$  such that  $F_n = k_n \delta_n$ . Tensile normal forces can develop for  $F_n \geq C_n$ , where  $C_n$  is the normal cohesion. Compressive forces  $F_n$  are counted positively, then  $C_n$  takes usually negative values. For  $F_n < C_n$  failure occurs and the contact is lost. For the tangential direction to the contact, the relation is elastic-perfectly plastic. In the elastic regime the shear contact force  $F_s$  is related to the incremental shear relative displacement  $\Delta u_s$  by  $F_s = -k_s \Delta u_s$ , where  $k_s$  is the shear stiffness. When  $|F_s| > F_n \tan(\Phi) + C_s$  (where  $\Phi$  and  $C_s$  are respectively the contact friction angle and the shear cohesion) sliding in tangential direction occurs and the contact becomes purely frictional (i.e.  $C_n = C_s = 0$ ). In this paper, the cohesive contact law is restricted to the case were  $-C_n = C_s = C$ .

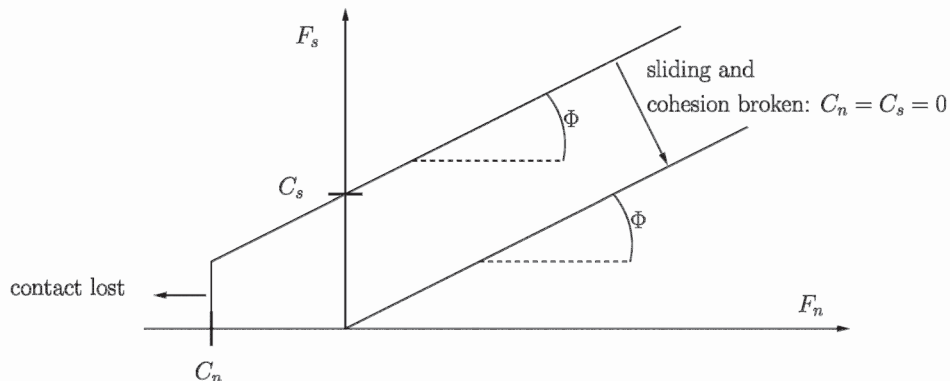


Figure 2: Cohesive inter-particle contact law used in the DE method.

At each time step of the DE method, resulting forces and torques applied at the center of each solid discs are deduced from the inter-particle forces computed with the contact law described above. New position, orientation, velocity and angular velocity of each solid particle are determined at the end of the DE time steps by carrying out an explicit time integration of equations of motion based on a Verlet scheme.

### II.3 Coupling of DE and LB methods

Since the basic ingredient of the LB method is the distribution function  $f(\vec{x}, t)$  representing fluid particles associated with a given momentum, the full coupling between both methods is realized by describing the exchange of momentum between the solid and the fluid phase.

As described in Figure 1-b, during the propagation stage of the LB method, a distribution function can encounter during its streaming, from one lattice node to another node along a given discrete direction  $i$ , a solid boundary (i.e. the boundary of a solid disk), such a direction is denoted  $\sigma i$ . The no-slip condition of fluid on the solid surface is described by applying the bounce-back rule consisting, roughly speaking, to inverse the direction of propagation of the distribution function. At the end of the propagation stage this latter come back to the node from where it left, but along the opposite direction  $-\sigma i$ . In general, the velocity of the solid boundary is not nil, such velocity should be taken into account to insure the no-slip condition and to describe the transfer of momentum from the solid phase to the fluid phase. Consequently, we used here the modified bounce-back rule writing:

$$f_{-\sigma i}(\vec{x}_{FB}, t + dt) = f_{\sigma i}(\vec{x}_{FB}, t^+) - 2\alpha_i \vec{V}_b \cdot \vec{e}_i, \quad (6)$$

where  $\vec{x}_{FB}$  represents a lattice node within the fluid domain with one or several discrete directions  $\sigma i$  pointing towards a solid boundary;  $\vec{V}_b$  is the velocity of the solid boundary estimated at the middle of the boundary link  $\sigma i$ ; and  $\alpha_i$  is a constant defined by:  $\alpha_i = 3 w_i \rho / C^2$ . The last term of equation (6) including  $\vec{V}_b$  represents the transfer of momentum from the solid to the fluid.

Action of fluid phase on solid phase is taken into account through the computation of hydrodynamic forces  $\vec{F}_h$  and torques  $\vec{T}_h$  acting on each solid disc boundary. For each boundary link  $\sigma i$ , time derivation of the momentum exchange between the two opposite directions of propagation ( $\sigma i$  and  $-\sigma i$ ) gives the contribution  $\vec{F}_\sigma$  of link  $\sigma i$  in the hydrodynamic force:

$$\vec{F}_\sigma(\vec{x}, t + \frac{1}{2} dt) = 2 \frac{h^2}{dt} \left[ f_{\sigma i}(\vec{x}_{FB}, t^+) - 2\alpha_i \vec{V}_b \cdot \vec{e}_i \right] \vec{e}_{\sigma i}. \quad (7)$$

Then the corresponding contribution  $\vec{T}_\sigma$  to the torque applied to the center of the solid disc writes:

$$\vec{T}_\sigma(\vec{x}, t + \frac{1}{2} dt) = \vec{r}_c \times \vec{F}_\sigma(\vec{x}, t + \frac{1}{2} dt), \quad (8)$$

where  $\vec{r}_c$  is the vector joining the center of the considered solid disc to the middle of the boundary link  $\sigma i$ . Total hydrodynamic force  $\vec{F}_h$  and torque  $\vec{T}_h$  acting on each solid disc are obtained by summing equations (7) and (8) over all the boundary links defining the disc boundary. Finally  $\vec{F}_h$  and  $\vec{T}_h$  are added, for each solid disc, to the force and torque resulting from inter-particle contact forces, to be taken into account, by this way, in the time integration of equations of motion performed in the DE cycle.

## III SIMULATION OF PIPING EROSION

### III.1 Numerical model

A two-dimensional granular assembly is created in a rectangular box by generating, randomly within the whole box, a very loose cloud of circular solid particles. At this stage, only the DE method is activated and the interstitial water is not described. The granular assembly is then compacted by growing solid particles (i.e. by expanding their radii). During the growing stage, cohesion between particles is switched off to facilitate particle reorganization. Once the granular assembly is compacted, particle cohesion is fixed to the desired value, and inlet and outlet water chamber, and central hole of initial diameter  $d_h$  are created by

removing the corresponding particles, such that only the hatched area represented in Figure 3-a is filled with the granular assembly. Finally, the whole simulation domain is discretized according to the D2Q9 model and the coupling with the LB method is activated. From now on, the granular assembly can be considered as fully saturated. Boundary conditions for the fluid are defined as follows: horizontal top and bottom walls of the box are treated as solid boundaries with no-slip condition; on vertical left and right walls are imposed pressure limit conditions in order to fix a water pressure gradient  $\Delta P$  between the inlet and the outlet and to create a water flow in the pre-existing hole from left to right (see Figure 3-a). Hence, this model can be seen as a quite simplified 2D representation of the hole erosion test (HET) [Wan, 2004].

By defining  $d$  as the mean diameter of two contacting discs, values of parameters related to the DE method are:  $k_n/d = 150 \cdot 10^6 \text{ N/m}^2$ ,  $k_s/k_n = 0.4$  and  $\Phi = 20^\circ$  (contact cohesion value is given further in next sections). Concerning the LB method:  $\nu = 1 \cdot 10^{-6} \text{ m}^2/\text{s}$ ,  $\tau = 1.1$  and the lattice counts 336000 nodes.

Under the action of the water flow, solid particles can be detached from the granular assembly and carried toward the outlet as shown in snapshots displayed in Figure 3-b. When a detached and transported solid particle reaches the right wall of the rectangular box (i.e. the right boundary of the simulation domain), the particle is removed from the simulation domain and the total mass of eroded solid  $M_e$  is increased of the mass of this particle.

A series of such numerical experiments have been performed to investigate the influence of two parameters, firstly the pressure gradient related to the hydraulic loading, and secondly the inter-particle cohesion related to the mechanical properties of the granular assembly.

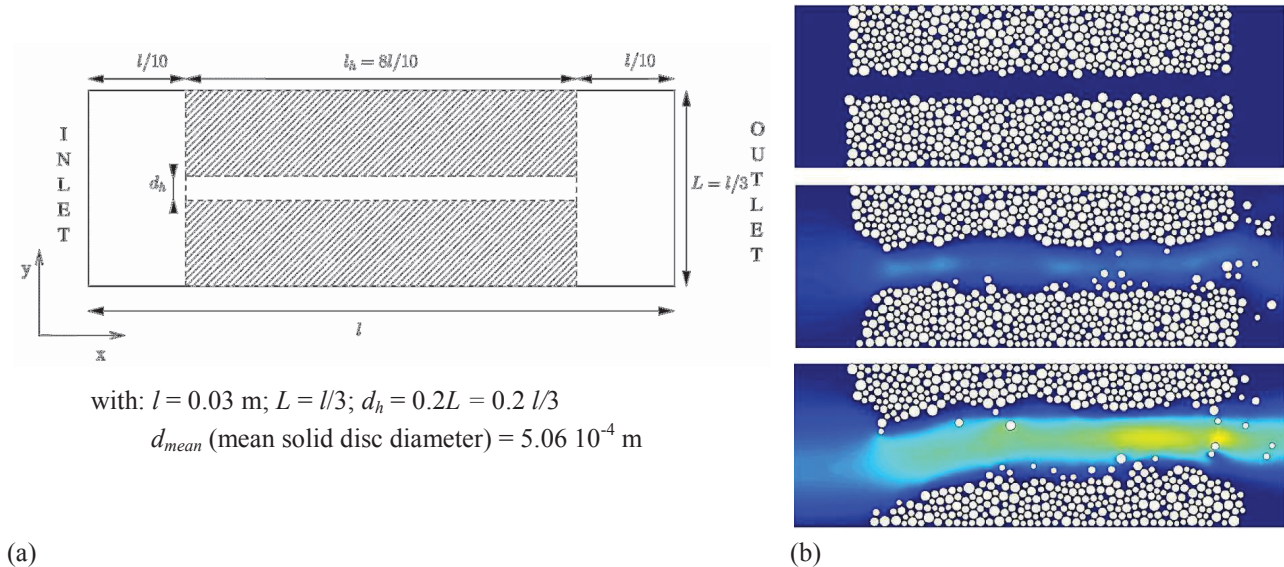


Figure 3: Sketch of the numerical model (a), and snapshots from the simulation of piping erosion for a pressure gradient  $\Delta P = 0.30 \text{ Pa}$  and a cohesion  $C/d = 0.253 \text{ N/m}$  (b).

### III.2 Simulation results and interpretation

Figure 4 shows time series of the ratio of eroded solid mass  $M_e(t)/M_0$  (where  $M_0$  is the total solid mass of the initial granular assembly), for an inter-particle cohesion  $C/d = 0.506 \text{ N/m}$  and for ten different values of pressure gradient, ranging from  $\Delta P = 0.01 \text{ Pa}$  to  $0.50 \text{ Pa}$ . For the lowest pressure gradient value, detachment of particles is not triggered, and the mass of eroded solid stay nil all along the simulation. For  $\Delta P > 0.01 \text{ Pa}$ , the rate of increasing of eroded mass grows with the value of the pressure gradient. For the highest values of  $\Delta P$ , the ratio of eroded solid mass reaches values close to unity during the simulation time, corresponding to the case where almost all the solid particles are eroded (some of the last particles stuck to the upper and bottom walls, cannot be detached by the water flow).

We suggest to interpret these numerical results as it is done classically for a HET [Wan, 2002], where the hydraulic shear stress  $\tau_h$  applied by the fluid on the hole surface is assumed to be the loading parameter leading the erosion regime. The erosion regime is characterised by the rate of eroded mass per unit pipe area  $\dot{e}$ , and it is linearly related to  $\tau_h$  such that:

$$\dot{e} = k_d (\tau_h - \tau_c) \quad \text{if } \tau_h > \tau_c, \tag{9}$$

where  $\tau_c$  is a critical shear stress (below which erosion is not triggered), and  $k_d$  is the erosion coefficient. These two last parameters should be typical of the erodability of the considered soil. From HET experimental results the hydraulic shear stress is commonly deduced by writing that pressure forces imposed at the inlet and the outlet of the apparatus are balanced by the shear force developed by the fluid on the lateral hole surface. However, since at any time of the simulation the fluid velocity field is given here by the LB method, in particular in the hole, the hydraulic shear stress  $\tau_h$  has been here computed from the fluid velocity gradient at the vicinity of the hole boundary:

$$\tau_h = \nu \rho_0 \frac{dV_x}{dy}, \tag{10}$$

where  $V_x$  represents a velocity cross profile averaged along the hole length [Lominé, 2012].

Figure 5 presents the plot of the erosion rate  $\dot{e}$  with respect to the hydraulic shear stress  $\tau_h$  for the numerical results displayed in Figure 4, thus for ten simulations performed with the same inter-particle cohesion ( $C/d = 0.506$  N/m) and different water pressure gradients. This plot shows that numerical data is quite well described by a linear approximation as suggested by equation (9). Consequently, values of a critical shear stress and of an erosion coefficient can be estimated for the considered numerical granular matter, independently of the water pressure gradient applied:  $\tau_c = 9 \cdot 10^{-4}$  Pa and  $k_d = 9.1$  s/m.

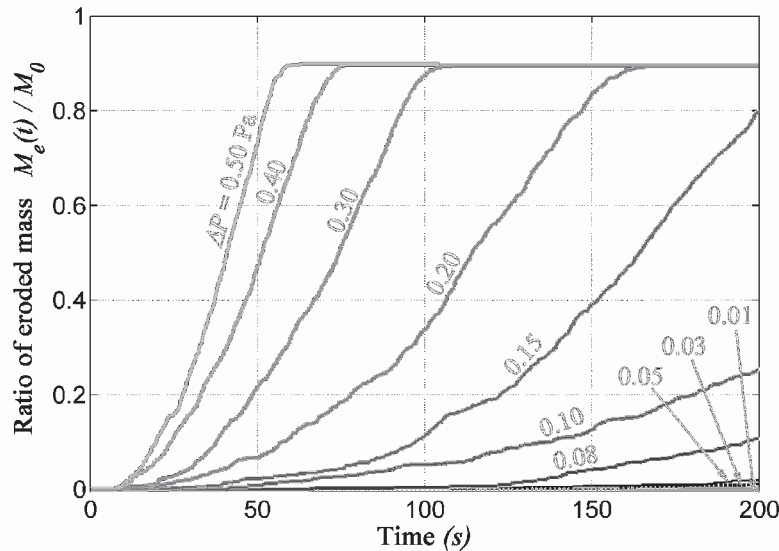


Figure 4: Time series of ratio of eroded mass for an inter-particle cohesion  $C/d = 0.506$  N/m.

### III.3 Influence of inter-particle cohesion on erosion

We consider now seven granular assemblies characterized each one by a different value of inter-particle cohesion ( $C/d = 0.152; 0.177; 0.253; 0.506; 1.27; 2.53$  and  $12.7$  N/m), all other parameters being kept constant. Each granular assembly have been numerically tested under six to ten water pressure gradient  $\Delta P$ . From the interpretation presented in Figure 5, critical shear stress  $\tau_c$  and erosion coefficient  $k_d$  were determined for each granular assembly (i.e. for each particle cohesion value). Figure 6 displays these values of  $\tau_c$  and  $k_d$  with respect to the inter-particle cohesion. For the highest cohesion value tested, corresponding to the last point of plots in Figure 6, erosion has not been triggered, even for the highest pressure gradient applied. Consequently the critical shear stress identified in this case represents only the highest hydraulic shear stress applied to the granular assembly and not a yield value above which erosion occurs. In addition, always in this case, the erosion coefficient cannot be determined as suggested in Figure 6-b.

Besides, for the three lowest values of cohesion, corresponding to the three first points of plots in Figure 6, the contact cohesion is broken in the bulk of the granular assembly at the initiation of the fluid flow (due to a water hammer), instead of being progressively broken for solid particles at the vicinity of the hole, as the diameter of this latter grows with the erosion of particles. Hence, in these cases, even if a small cohesion is

initially introduced in the granular packing, this one is quasi immediately removed in the whole packing as soon as the flow starts. Then the granular assembly behaves essentially as a cohesionless material and the value of  $\tau_c$  for the three lowest cohesion values (Figure 6-a) is more likely representative of a cohesionless granular assembly than a weakly cohesive material.

Despite these two remarks, the erosion coefficient  $k_d$  seems independent of the cohesion whereas the critical shear stress  $\tau_c$  seems directly affected by the cohesion of the granular assembly; even if we cannot conclude, from the numerical data presented in this paper, about the kind of the relation (linear or not) between cohesion and  $\tau_c$ .

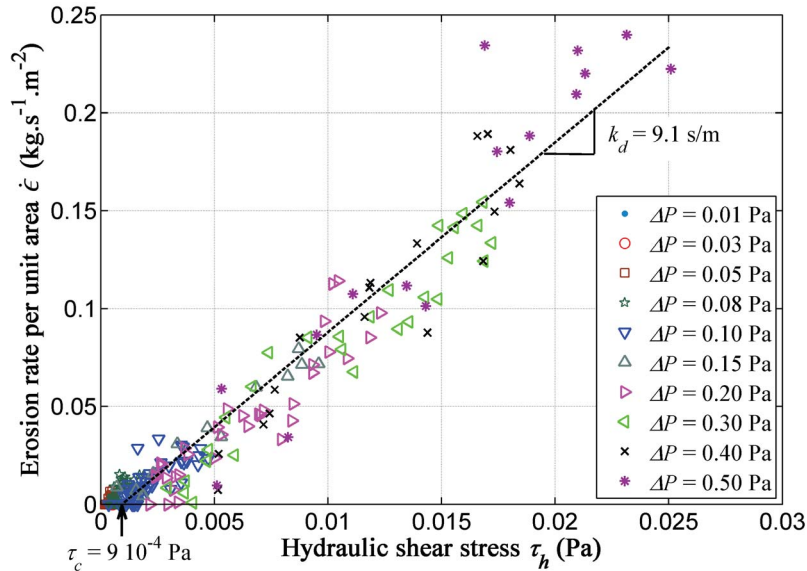


Figure 5: Erosion rate as a linear function of hydraulic shear stress.

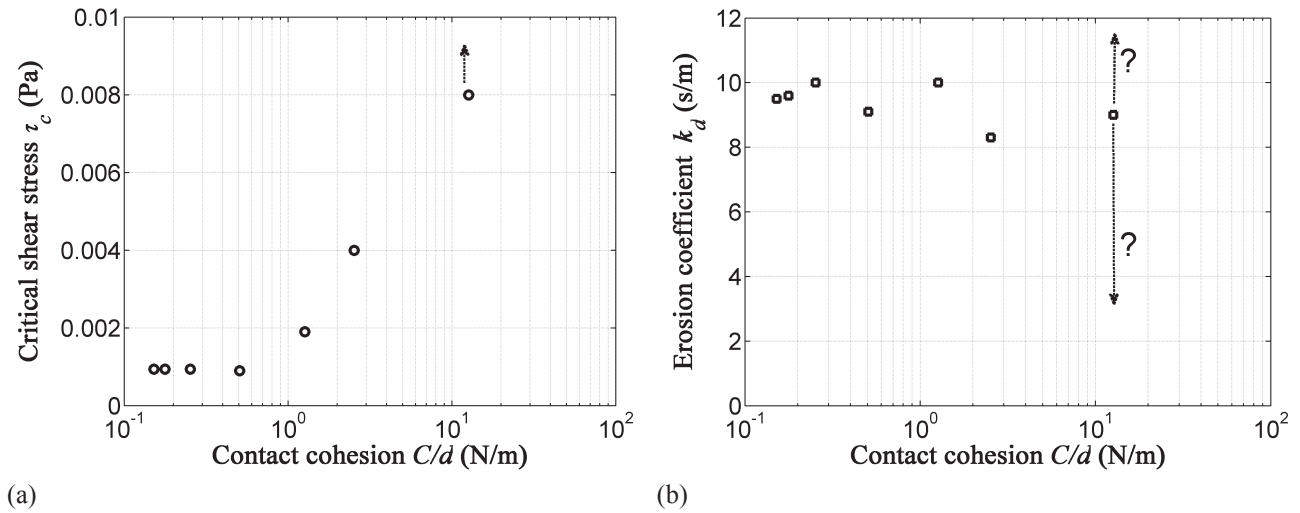


Figure 6: Influence of inter-particle contact cohesion on critical hydraulic shear stress (a) and erosion rate (b).

#### IV CONCLUSIONS

The lattice Boltzmann–discrete element coupled method appears as an adapted tool to describe, at the microscopic scale, fluid-solid interactions in granular matter. Few hypotheses are coming with such method, avoiding any phenomenological description, and limiting the number of mechanical parameters (there are five here, the fluid viscosity, the normal and shear contact stiffnesses, the contact cohesion between two solid particles, and finally the inter-particle friction angle). However the computational cost, due to the necessity of a sufficiently fine fluid lattice, can be important, and limitations can appear with respect to the maximum water velocity that one aims to describe and the assumption of fluid quasi-incompressibility.

The application of this coupled method to piping erosion presented here is quite simplified. The description of the solid phase as a granular assembly made of discs can seem far from a real soil, as for instance a clayey sand. However, solid discs used here do not represent necessarily an elementary soil particle but can be seen as an aggregate, of clay around a sand grain for instance. Concerning the fluid phase, for the sake of simplicity, we voluntarily limited the description to laminar flows in a first time. This restriction can also appear as a gap with respect to real flows, possibly encounter in piping erosion problem. However turbulence models have been developed for the LB method and could be introduced in such simulations [Feng, 2007].

Despite limitations discussed here above, results presented in this paper are encouraging. A linear dependency of the erosion rate on the hydraulic shear stress, as usually observed experimentally, is retrieved from the direct simulations performed and with the only mechanical parameters listed above. Influence of contact cohesion on critical shear stress and erosion coefficient may be intuitively described. Nevertheless this result gives an example of the way by which this coupled numerical method could be useful. The objective here is not to reach a quantitative prediction of the piping erosion, but to give a qualitative description allowing to clearly identify the relevant local parameters (related to the solid phase and the fluid phase) involved in soil erosion phenomena.

## V ACKNOWLEDGMENTS AND THANKS

The scientific context and the financial support provided by the French Region Pays de la Loire through the EMERMOD project are gratefully acknowledged.

## VI REFERENCES AND CITATIONS

Bhatnagar P.L., Gross E.P., & Krook M. (1954) – A Model for Collision Processes in Gases. I. Small Amplitude Processes in Charged and Neutral One-Component Systems. *Physical Review*, **94**(3): 511-525.

Cundall P., & Strack O. (1979) – A discrete numerical model for granular assemblies. *Geotechnique*, **29**(1): 47-65.

Feng Y.T., Han K., & Owen D.R.J. (2007) – Coupled lattice Boltzmann method and discrete element modelling of particle transport in turbulent fluid flows: Computational issues. *Int. J. for Numer. Meth. Eng.*, **72**(9): 1111-1134.

Lominé F., Scholtès L., Sibille L., & Poullain P. (2012) – Modelling of fluid-solid interaction in granular media with coupled lb/de methods: application to piping erosion. *Int. J. Numer. Anal. Meth. Geomech.*, DOI 10.1002/nag.1109 **(In press)**.

Qian Y.H., D’Humières D., & Lallemand P. (1992) – Lattice BGK Models for Navier-Stokes Equation. *EPL (Europhysics Letters)*, **17**(6): 479-484.

Šmilauer V., Catalano E., Chareyre B., Dorofeenko S., Duriez J., Gladky A., Kozicki J., Modenese C., Scholtès L., Sibille L., Stránský J., & Thoeni K. (2010) – *Yade Documentation (V. Šmilauer, ed.)*, *The Yade Project, 1st ed.*. <http://yade-dem.org/doc/>.

Succi S. (2001) – *The lattice Boltzmann equation for fluid dynamics and beyond*. Oxford: University Press.

Tsai J.-C., Voth G., & Gollub J. (2003) – Internal granular dynamics, shear-induced crystallization, and compaction steps. *Physical Review Letters*, **91**: 064301.

Wan C.F., & Fell, R. (2004) – Investigation of erosion rate of soils in embankment dams. *Journal of Geotechnical and Geoenvironmental Engineering*, **130**(4): 373-380.

Wan C.F., & Fell R. (2002) – *Investigation of internal erosion and piping of soils in embankment dams by the slot erosion test and the hole erosion test. Technical Report R-412*. Sydney: University of New South Wales.